Sustainable Energy & Fuels



PAPER

View Article Online
View Journal | View Issue



Cite this: Sustainable Energy Fuels, 2024, **8**, 5449

Received 20th June 2024

Accepted 9th October 2024 DOI: 10.1039/d4se00820k

rsc.li/sustainable-energy

Pressure-swing absorption and desorption behaviours of ammonia in bis(trifluoromethylsulfonyl)amide salts†

Manabu Tokushige, Ryota Fujisawa and Junichi Ryu **D**

The absorption and desorption behaviours of NH₃ in bis(trifluoromethylsulfonyl)amide (TFSA) salts were investigated using the pressure-swing method. The effects of cation species and temperature on the NH₃ absorption behaviour of four TFSA salts, namely, Na[TFSA], K[TFSA], Mg[TFSA]₂, and Ca[TFSA]₂, were evaluated. NH₃ was absorbed by these solid TFSA salts, and high NH₃ desorption was observed for Na [TFSA] at 473 K and K[TFSA] at 300 K. The NH₃ absorption behaviour varied with the cation of the TFSA salt. Crystallographic refinement showed that the crystal lattice of Na[TFSA] expanded and contracted along the c-axis upon NH₃ absorption and desorption, respectively, indicating the coordination of NH₃ molecules with cation sites between the lattice layers. For the alkaline-earth metal TFSA salts, NH₄[TFSA] and amide compounds (Mg(NH₂)₂ or Ca(NH₂)₂) were formed after NH₃ absorption. Therefore, two absorption processes—coordination and dissociation of NH₃—occurred in the TFSA salts.

1 Introduction

For over a century, ammonia (NH₃) has been produced, addressing food security as a nitrogen-based fertilizer and securing our livelihood by serving as a feedstock for various chemical products.^{1,2} However, conventional production (via the Haber-Bosch process) requires a substantial amount of energy because of the requirement of high pressures (5-20 MPa) and temperatures ranging from 673 to 873 K for the synthesis of NH₃.¹⁻⁷ In contrast, Aika et al.⁸⁻¹¹ proposed an NH₃ production system using a Ru catalyst and selective NH3 absorber. Conventional separations of NH3 involve cryogenic condensation below 240 K,12-14 even though NH3 is obtained from the synthetic reactors at high temperatures (~473 K). ^{15,16} The cryogenic condensation of high-temperature gases containing NH3 and reactants (H₂ and N₂) requires a substantial amount of energy, and the subsequent reheating to return the reactant gases to the synthetic reactor results in energy loss. 10,11,17-19 The selective NH3 absorber reduces energy losses during NH3 separation, and swift NH₃ separation using absorbers enables the synthesis of NH₃ under mild conditions such as lower pressures and temperatures because the production rate of NH₃ is improved by the prompt circulation of reactant gases. 11,17-23 Liu and Aika¹⁸⁻²⁰ confirmed that mixed halide compounds such as CaCl2 and CaBr2 exhibited a high NH3 storage capacity and established the production system for NH3 using these

Graduate School of Engineering, Chiba University, Chiba 263-8522, Japan. E-mail: jryu@chiba-u.jp

absorbers (the absorber-enhanced Haber-Bosch process). Malmali et al.24-31 demonstrated that NH3 was economically and efficiently produced using the absorber-enhanced Haber-Bosch process. They separated NH₃ using halides as the absorber at 453 K and 0.6 MPa and confirmed that the production of NH₃ was determined by the circulation rate of reactant gases. The absorber-enhanced Haber-Bosch process reduces the cost and energy consumption required to produce NH3. Although various types of absorbers have been investigated,17-41 the operation of the absorber-enhanced Haber-Bosch process has still not been optimized because of the complex NH3 absorption and desorption mechanisms, such as the discrete stoichiometry of ammine compounds and slow NH3 desorption.37 NH3 is absorbed into halides through the coordination of NH3 with the cation and formation of ammine complexes. Subsequently, it desorbs from halides by dissociation of ammine complexes and diffusion of NH3 into the gas phase.19 The formation and dissociation of ammine complexes are relatively slow. The rates of formation and dissociation of ammine complexes are predominantly determined by the heat of reaction (enthalpy change), which serves as the energy barrier for the absorption and desorption of NH3. The dissociation of many ammine compounds requires a substantial heat of reaction ($\sim 100 \text{ kJ mol}^{-1}$) (Table 1), resulting in a low NH₃ desorption rate. This implies that the rate and efficiency of NH₃ production are enhanced by improving the NH3 desorption function of the absorber. Malmali et al. desorbed NH₃ from an absorber using the temperature-swing method (TSA). Meanwhile, we have developed a high-temperature NH3 absorber to separate NH3 obtained at 473 K from the synthetic reactor. This selective absorber reduced the heat loss during cooling and reheating

[†] Electronic supplementary information (ESI) available. See DOI: https://doi.org/10.1039/d4se00820k

Table 1 NH₃ absorption functions of each absorber at the standard state

| Absorber | Ammine compounds | Storage capacity | Enthalpy change | Reference |
|-------------------|---|--|----------------------------|-----------|
| $MgCl_2$ | Mg(NH ₃)Cl ₂ | $11 \; \mathrm{mmol} \; \mathrm{g}^{-1}$ | −93 kJ mol ^{−1} | 32 |
| 0 2 | $Mg(NH_3)_2Cl_2$ | 21 mmol g^{-1} | -85 kJ mol^{-1} | |
| | $Mg(NH_3)_6Cl_2$ | 63 mmol g^{-1} | _ | |
| CaCl ₂ | Ca(NH ₃)Cl ₂ | 9 mmol g^{-1} | -81 kJ mol^{-1} | |
| | $Ca(NH_3)_2Cl_2$ | 18 mmol g^{-1} | -74 kJ mol^{-1} | |
| | $Ca(NH_3)_4Cl_2$ | 37 mmol g^{-1} | −83 kJ mol ^{−1} | |
| | Ca(NH ₃) ₈ Cl ₂ | 72 mmol g^{-1} | -164 kJ mol^{-1} | |
| CaBr ₂ | Ca(NH ₃)Br ₂ | 5 mmol g^{-1} | −71 kJ mol ^{−1} | |
| _ | $Ca(NH_3)_2Br_2$ | 10 mmol g^{-1} | −79 kJ mol ^{−1} | |
| | $Ca(NH_3)_6Br_2$ | 20 mmol g^{-1} | -182 kJ mol^{-1} | |
| | $Ca(NH_3)_8Br_2$ | 40 mmol g^{-1} | -83 kJ mol ⁻¹ | |
| [emim][TFSA] | | 42 mmol g^{-1} @ 1.0 MPa | −7 kJ mol ^{−1} | 33 |

NH3 and reactant gases, as NH3 is easily separated using the pressure-swing method (PSA). Bis(trifluoromethylsulfonyl) amide (TFSA) salts, which are amide salts with imino groups, have several desirable properties such as nonvolatility, nonflammability, high thermal stability, absorption of NH₃, and low solubilities of H2 and N2.42-55 For example, NH3 dissolved in 1-ethyl-3-methyl-imidazolium ([emim]) [TFSA] at 300 K has solubilities of 42.3, 3.36, and 0.527 mmol g^{-1} at 1.0, 0.4, and 0.1 MPa, respectively.33 The heat of dissolution of NH3 in this TFSA salt (\sim 10 kJ mol⁻¹) is lower than that required for the formation of ammine complexes (~100 kJ mol⁻¹), which indicates that the rates of absorption and desorption of NH3 in this TFSA salt are higher than those in halides. Furthermore, TFSA anions can interact with metal centers either as bidentate ligands or by bridging several metal centers.⁵⁶ Consequently, alkaline and alkaline-earth metal TFSA salts exhibit layered structures in the solid state, as shown in Fig. 1.56-59 Because the NH₃ molecule coordinates with a cationic site, 19,23 these solid TFSA salts are expected to absorb NH3 molecules at each cationic site between the lattice layers. In this study, we

investigated the absorption/desorption behaviour of NH_3 in solid TFSA salts at 473 and 300 K. For four TFSA salts, namely $\mathrm{Na[TFSA]}$, $\mathrm{K[TFSA]}$, $\mathrm{Mg[TFSA]}_2$, and $\mathrm{Ca[TFSA]}_2$, the effects of cation species and temperatures on the NH_3 absorption behaviour were evaluated using crystallographic and kinetic analyses.

2 Experimental

The NH₃ absorption/desorption cycles of the four TFSA salts were measured using a magnetic suspension balance (MSB-143, Rubotherm GmbH, Germany) and the pressure-swing method. Commercially available TFSA salts such as Na[TFSA] (purity: >98%; SO989), K[TFSA] (purity: >98%; B2543), Mg[TFSA]₂ (purity: >97%; M2861), and Ca[TFSA]₂ (purity: >97%; C3263) were purchased from Tokyo Chemical Industry Co. Ltd. The experimental setup is described in a separate paper. The TFSA powder sample (\sim 300 mg) was placed in a Pt basket (\varnothing 20 mm \times 50 mm) hanging from a magnet, and the basket was suspended inside the furnace *via* the magnetic force. Before initiating the

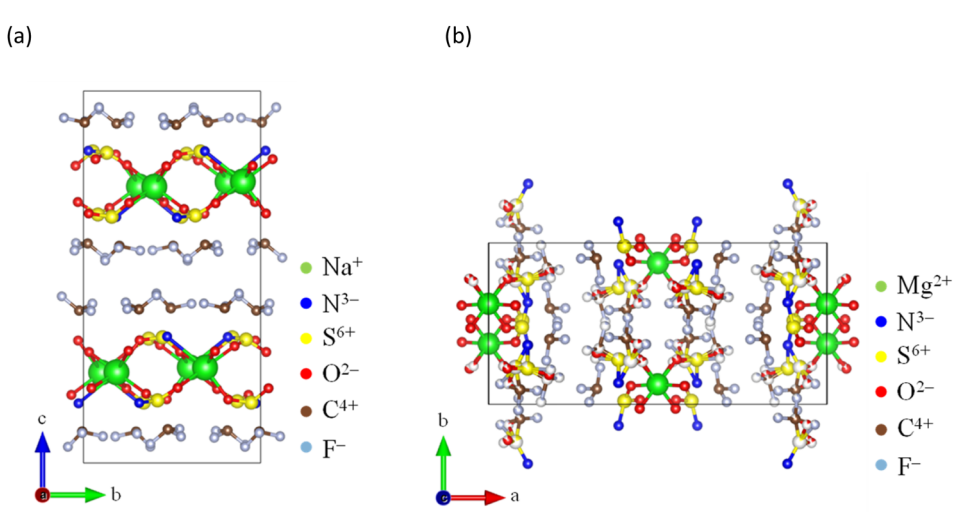


Fig. 1 Crystal structures of TFSA salts: (a) Na[TFSA]⁵⁷ and (b) Mg[TFSA]₂.⁵⁹

NH₃ absorption/desorption cycle, the TFSA sample was dehydrated at 493 K for 1 h under vacuum as pretreatment. After dehydration, pure NH3 gas (99.9% purity; Resonac Holdings Corp., Tokyo, Japan) was introduced into the furnace. NH₃ absorption into the sample was conducted under a NH3 gas pressure of 0.5 MPa for 2 h (pressure-swing absorption), whereas NH3 desorption was conducted under a NH3 gas pressure of 0.1 MPa for 3 h (pressure-swing desorption). The pressure of NH₃ was controlled by the temperature of the NH₃ tank immersed in an ethanol bath. After NH3 absorption/ desorption cycles, the sample powders were characterized using X-ray diffraction (XRD; Ultima IV, Rigaku Corp., Japan). XRD data were obtained in the 2θ range of 5-90° at room temperature, with a step interval of 0.01°, using Cu-Kα radiation, calibrated with Si powder. The obtained diffraction patterns were analysed via the entire powder pattern fitting method, 61,62 using PDXL (Rigaku Corp.) and split pseudo-Voigt functions. The corresponding crystal structures were visualized using VESTA.63

3 Results and discussion

Absorption and desorption behaviours of ammonia

Typical NH₃ absorption/desorption cycles for Na[TFSA] at 473 K are shown in Fig. 2. Na[TFSA] exhibits a stable NH₃ absorption capacity at 473 K and all pressures (0.1 and 0.5 MPa of NH₃ gas). The absorption capacity (C_{abs}) and desorption capacity (C_{des}) of NH₃ are defined as follows:

$$C_{\rm abs} = \frac{W_{\rm abs} - W_{\rm s}}{W_{\rm s}} \times \frac{1}{M_{\rm NH_3}} \tag{1}$$

$$C_{\text{des}} = \frac{|W_{\text{des}} - W_{\text{abs}}|}{W_{\text{s}}} \times \frac{1}{M_{\text{NH}_3}} \tag{2}$$

where W_s is the sample weight before the NH₃ absorption/ desorption cycle, W_{abs} is the sample weight after the absorption cycle, and W_{des} is the sample weight after the desorption cycle. $M_{\rm NH_2}$ is the molar weight of NH₃. The absorption/ desorption rates (v_{abs} and v_{des}) are defined as the rates at which 80% of the capacity is achieved in each cycle. Na[TFSA] absorbs NH₃ ($C_{abs} = 3.05 \text{ mmol g}^{-1}$) and exhibits the highest NH₃ desorption capacity ($C_{\text{des}} = 2.83 \text{ mmol g}^{-1}$) among the four TFSA salts. This result indicates that almost all of the

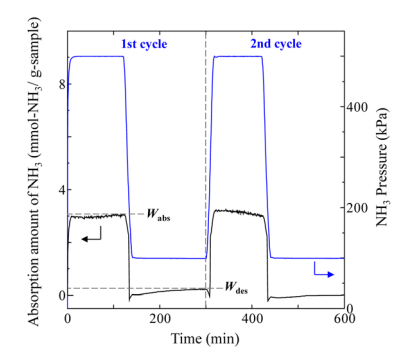


Fig. 2 Typical NH₃ absorption/desorption cycles of Na[TFSA] at 473 K.

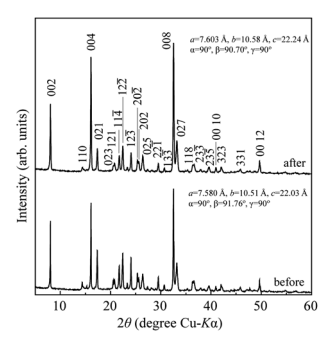


Fig. 3 XRD patterns of Na[TFSA] before and after NH₃ absorption/ desorption cycles at 473 K.

absorbed NH₃ in Na[TFSA] can be collected via PSA. The XRD patterns of the Na[TFSA] powder before and after the NH3 absorption/desorption cycles are shown in Fig. 3. The observed diffraction patterns are consistent with Na[TFSA] with a monoclinic P21/n structure, 57 exhibiting crystal orientation and expansion along the c-axis after the absorption/ desorption cycles. This result suggests that the NH3 molecules are absorbed between the lattice layers of Na[TFSA]. As shown in Fig. 4, the NH₃ absorption behaviour varies based on the cation species of the TFSA salts. The results of the NH₃ absorption/desorption cycles for each TFSA sample are summarized in Table 2. Only a small amount of NH3 is absorbed by K[TFSA] (Fig. 4a). Among the TFSA salts, Mg [TFSA]₂ exhibits the highest NH₃ absorption capacity ($C_{abs} =$ 8.29 mmol g⁻¹) at 473 K, although the desorption capacity is low ($C_{\text{des}} = 1.22 \text{ mmol g}^{-1}$) (Fig. 4b and Table 2). The C_{abs} values increase in the order of Mg[TFSA]₂ > Ca[TFSA]₂ > Na [TFSA]. This result is consistent with that reported by Liu and Aika.23 They identified the absorption site of NH3 and clarified the absorption mechanism with alkaline or alkaline-earth metal cations using a thermal conductivity detector and FT-IR spectroscopy. NH₃ is absorbed at these cation sites by three processes: coulombic attraction, the formation of ammonium ions, and the formation of ammine complexes in cation sites. Therefore, it is likely that NH3 is absorbed at the alkaline or alkaline-earth metal cations of the TFSA salts. Based on the results of Liu and Aika,23 NH3 molecules are absorbed through the coulombic attraction between alkaline or alkaline-earth metal cations and the nitrogen anions of NH_3 . Therefore, C_{abs} varies with the surface charge density of the alkaline or alkaline-earth metal cations. After the NH₃ absorption/desorption cycle at 473 K, the solid Mg[TFSA]₂ liquefies (Fig. 5b). This liquefaction decreases the NH₃ desorption from Mg[TFSA]2. The XRD pattern of the solidified Mg[TFSA]₂ sample at room temperature is shown in Fig. 6a. The observed diffraction pattern is assigned to NH₄[TFSA] with an orthorhombic Pnab structure65 and Mg(NH2)2 with a cubic $I4_1/acd$:2 structure, 66 indicating that the Mg²⁺ cations are displaced by NH₄⁺ cations as follows:

$$Mg[TFSA]_2 + 4NH_3 \rightarrow 2NH_4[TFSA] + Mg(NH_2)_2$$
 (3)

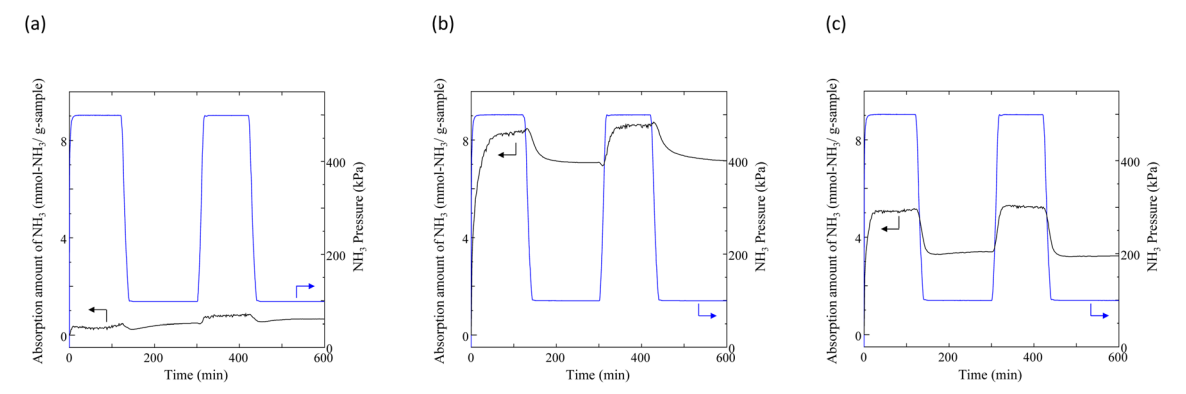


Fig. 4 Typical NH₃ absorption/desorption cycles for TFSA salts at 473 K: (a) K[TFSA], (b) Mg[TFSA]₂, and (c) Ca[TFSA]₂.

Table 2 NH₃ absorption/desorption measurements at 473 K

| TFSA | Cycle | Absorption capacity, C_{abs} (mmol g^{-1}) | Absorption rate, v_{abs} (mmol $g^{-1} \min^{-1}$) | Desorption capacity, C_{des} (mmol g^{-1}) | Desorption rate, v_{des} (mmol g ⁻¹ min ⁻¹) |
|---------------------------|-------|---|---|--|---|
| Na[TFSA] | 1st | 3.05 | 0.81 | 2.83 | 0.17 |
| | 2nd | 3.03 | 0.19 | 3.03 | 0.20 |
| $Mg[TFSA]_2$ | 1st | 8.29 | 0.36 | 1.22 | 0.02 |
| | 2nd | 8.66 | _ | 1.51 | 0.02 |
| Ca[TFSA] ₂ | 1st | 5.19 | 0.47 | 1.74 | 0.07 |
| . 12 | 2nd | 5.18 | 0.32 | 1.95 | 0.09 |
| Na-Y zeolite ^a | 1st | 5.08 | 4.14 | 2.18 | 0.10 |
| | 2nd | 5.45 | 0.59 | 2.09 | 0.09 |

^a The results of Na-Y zeolite were referred from ref. 64.

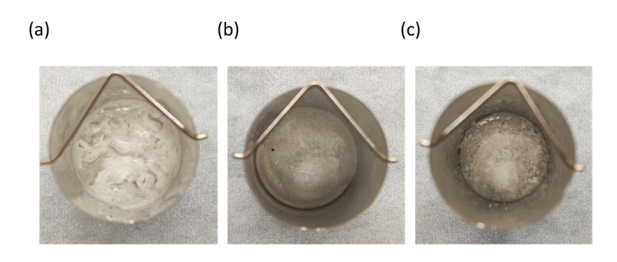


Fig. 5 Photographs of TFSA salts after the NH₃ absorption/desorption cycles at 473 K: (a) Na[TFSA], (b) Mg[TFSA]₂, and (c) Ca[TFSA]₂ in the Pt basket (ø 20 mm).

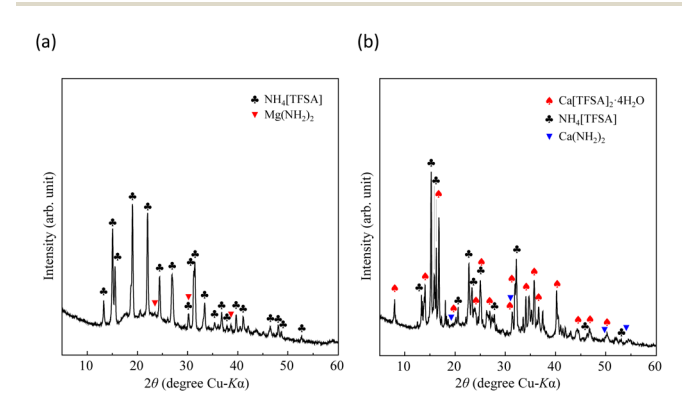


Fig. 6 XRD patterns of alkaline-earth metal TFSA salts after NH₃ absorption/desorption cycles at 473 K: (a) Mg[TFSA]₂ and (b) Ca[TFSA]₂.

Liquefaction of solid salts that absorb excessive NH3 has already been reported. 40,60,67 Ammonium (NH4+) cations and amide (NH₂⁻) anions have been observed in bis(fluorosulfonyl) amide (FSA) salts after NH₃ absorption, and the FSA salts were liquefied by formation of a eutectic mixture among them.60 Similarly, the liquefaction of the Mg[TFSA]₂ salt can be explained by a eutectic phenomenon. This indicates that the NH₃ molecule coordinates with the Mg²⁺ cation between the lattice layers and dissociates in the Mg[TFSA]₂ salt. Therefore, two absorption processes, coordination and dissociation, occur in Mg[TFSA]2, as shown in Fig. 7. The XRD pattern of the Ca [TFSA]₂ sample shows phases of Ca[TFSA]₂,⁵⁷ NH₄[TFSA], and

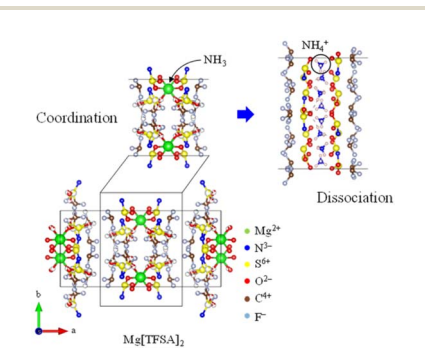
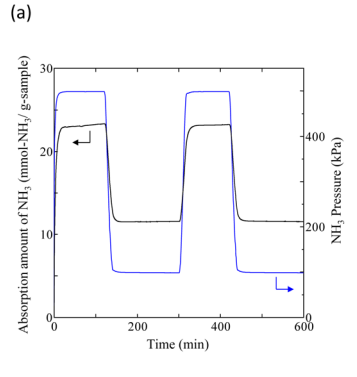
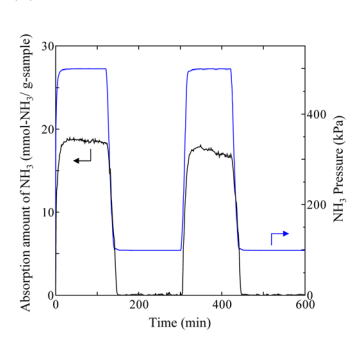
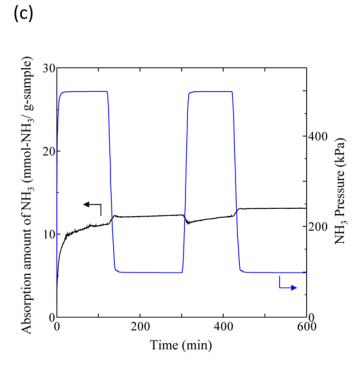


Fig. 7 Absorption mechanism of NH₃ into TFSA salt.





(b)



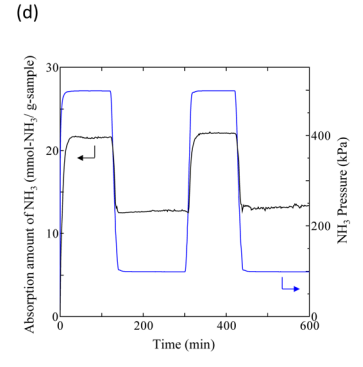


Fig. 8 Typical NH₃ absorption/desorption cycles in various TFSA salts at 300 K: (a) Na[TFSA], (b) K[TFSA], (c) Mg[TFSA]2, and (d) Ca[TFSA]2.

Ca(NH₂)₂ (ref. 68) (Fig. 6b). Therefore, in addition to Mg[TFSA]₂, the above mentioned two absorption processes occur in Ca [TFSA]₂. To evaluate the temperature dependence of the NH₃ absorption/desorption behaviour of the solid TFSA salts, NH₃

absorption/desorption cycles were examined at 300 K (Fig. 8 and Table 3). Cabs was higher at lower temperatures. At 300 K, Na [TFSA] exhibited the highest Cabs. K[TFSA] absorbed NH3 under 0.5 MPa and showed the high desorption function of NH₃. All absorbed NH₃ was desorbed from K[TFSA] under 0.1 MPa. The difference of NH₃ absorption behaviours by temperature can be attributed to the NH3 molecular motion. The NH3 molecular motion was vigorous and C_{abs} decreased at high temperature (473 K). On the other hand, the absorbed NH₃ did not desorb from Mg[TFSA]₂ at 300 K (Fig. 8b). The crystal lattice of Na[TFSA] shrank after NH₃ absorption/desorption cycles at 300 K (Fig. 10a), implying that the Na[TFSA] lattice expanded during NH₃ absorption and shrank during NH₃ desorption. Mg[TFSA]₂ remained in the solid state after NH3 absorption/desorption cycles at 300 K (Fig. 9). The XRD pattern of the Mg[TFSA]₂ sample after cycling at 300 K showed both Mg[TFSA]2 and NH₄[TFSA] phases (Fig. 10b). The Mg²⁺ cations in Mg[TFSA]₂ were not entirely displaced by NH₄⁺ cations. Therefore, the absorption process was limited by the dissociation of NH₃ in Mg [TFSA]₂ at 300 K. Regarding kinetics, the NH₃ absorption rate of Na[TFSA] was similar to its NH₃ desorption rate. Na[TFSA] exhibited the highest v_{abs} and v_{des} among the TFSA samples. v_{abs} and $v_{\rm des}$ values were higher at lower temperatures. In addition, although all TFSA salts except K[TFSA] showed similar NH3 absorption behaviour at 473 K, they exhibited different behaviours at 300 K (Fig. 11). This was caused by the difference in the absorption processes; the absorption into the TFSA salts was limited by the dissociation of NH₃ in the salts. The double exponential model used to evaluate the kinetics of the two absorption processes is as follows:69-71

$$W(t) = A_{\rm crd} \exp(-k_{\rm crd}t) + A_{\rm dis} \exp(-k_{\rm dis}t) + C \tag{4}$$

where W(t) is the change in sample weight over time t after the start of NH₃ absorption, and k_{crd} and k_{dis} are the rate constants for the coordination and dissociation of NH3, respectively.

 $A_{\rm crd}$ and $A_{\rm dis}$ are the frequency factors for the coordination and dissociation, respectively, and C is a constant. The first and second terms on the right side of eqn (4) correspond to the coordination and dissociation of NH3 in the TFSA salts, respectively. The kinetic parameters were obtained by fitting the initial stage of the NH3 absorption curves for each TFSA salt (Fig. 11a and c) using eqn (4), and the values are listed in Tables 4 and 5. The least-squares fitting results are shown in Fig. S1 and S2.† The rate constants of the coordination step are considerably higher than those of the dissociation step ($k_{\rm crd}$ > $k_{\rm dis}$), confirming dissociation to be the rate-determining step. The value of $k_{\rm crd}$ increases and that of $k_{\rm dis}$ decreases with decreasing temperature. For Ca[TFSA]₂ at 300 K, $k_{\rm dis}$ is significantly small, suggesting that the dissociation of NH3 in Ca [TFSA]₂ is slow at 300 K. Therefore, coordination is the dominant process, whereas dissociation progressed to a lesser extent in the Ca[TFSA]₂ salt.

3.2 Comparison of TFSA salts with zeolites

In our previous study,64 NH3 adsorption and desorption behaviours on zeolites at 473 K were observed by PSA cycling

Table 3 NH₃ absorption/desorption measurements at 300 K

| TFSA | Cycle | Absorption capacity, $C_{\rm abs}$ (mmol g ⁻¹) | Absorption rate, v_{abs} (mmol $g^{-1} \min^{-1}$) | Desorption capacity, C_{des} (mmol g ⁻¹) | Desorption rate, v_{des} (mmol $g^{-1} min^{-1}$) |
|-----------------------|-------|--|---|---|--|
| Na[TFSA] | 1st | 23.34 | 3.61 | 11.77 | 0.53 |
| . , | 2nd | 23.26 | 1.29 | 11.72 | 0.52 |
| K[TFSA] | 1st | 18.48 | 2.56 | 18.37 | 0.63 |
| | 2nd | 17.02 | 0.87 | 17.02 | 0.60 |
| Ca[TFSA] ₂ | 1st | 21.64 | 2.05 | 8.92 | 0.57 |
| | 2nd | 22.07 | 1.25 | 8.76 | 0.57 |
| | | | | | |



Fig. 9 A photograph of the $Mg[TFSA]_2$ sample after NH_3 absorption/desorption cycles at 300 K. $Mg[TFSA]_2$ sample in the glass bottle (\emptyset 24 mm, 10 mL).

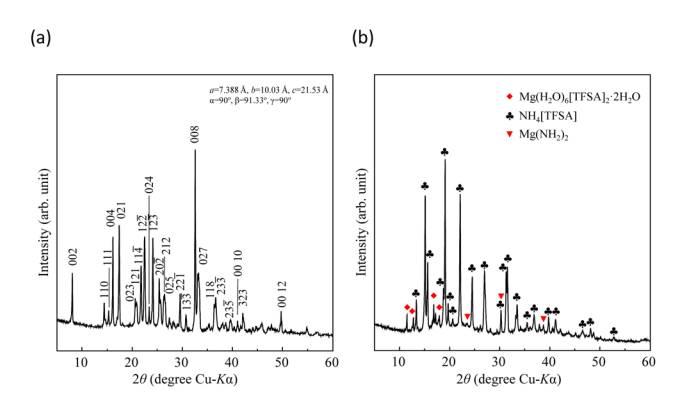


Fig. 10 XRD patterns of TFSA salts after NH $_3$ absorption/desorption cycles at 300 K: (a) Na[TFSA] and (b) Mg[TFSA] $_2$.

(0.1-0.5 MPa), and their stability for NH₃ storage was confirmed. Typical NH₃ adsorption and desorption behaviours of Na-Y and A-4 zeolites at 473 K are shown in Fig. S3.† As shown in Table 2, although the NH3 adsorption capacity of the Na-Y zeolite ($C_{ads} = 5.08 \text{ mmol g}^{-1}$, 7.16 mol m⁻³) is higher than that of Na[TFSA] ($C_{abs} = 3.05 \text{ mmol g}^{-1}$, 7.13 mol m⁻³), the NH_3 desorption capacity of the Na-Y zeolite ($C_{des} = 2.18$ mmol g^{-1} , 3.07 mol m⁻³) is lower than that of Na[TFSA] ($C_{des} =$ 2.83 mmol g^{-1} , 6.62 mol m^{-3}). Additionally, the NH₃ desorption rate of Na–Y zeolite ($v_{des} = 0.10 \text{ mmol g}^{-1} \text{ min}^{-1}$) is lower than that of the Na[TFSA] salt ($v_{\text{des}} = 0.17 \text{ mmol g}^{-1} \text{ min}^{-1}$). Hence, the NH₃ desorption function of the Na-Y zeolite is less than that of Na[TFSA]. These results indicate that zeolites contain noncollectible NH3 during this PSA cycle (0.1-0.5 MPa, collection ratio: 43%). In contrast, almost all the NH₃ absorbed by the Na [TFSA] salt is collected (collection ratio: 93%). Therefore, the high NH3 desorption function is an advantage of NH3 separation using TFSA salts. Finally, to evaluate the durability of the Na[TFSA] for NH₃ absorption/desorption at 473 K, five NH₃ absorption/desorption cycles were conducted (Fig. 12a). Stable NH₃ absorption/desorption behaviours were observed, although the baseline of balance was drifted by multiple changes in NH₃ pressure. From the cycle performance of the NH₃ desorption capacity as a working capacity (Fig. 12b), it was confirmed that Na[TFSA] absorbed and desorbed NH3 in stably and repeatably. Furthermore, even after five NH3 absorption/ desorption cycles, Na[TFSA] remained as a sold-state and no other compounds such as NH₄[TFSA] were observed (Fig. 12c). From these results, the durability of the Na[TFSA] was confirmed for NH₃ absorption/desorption at 473 K.

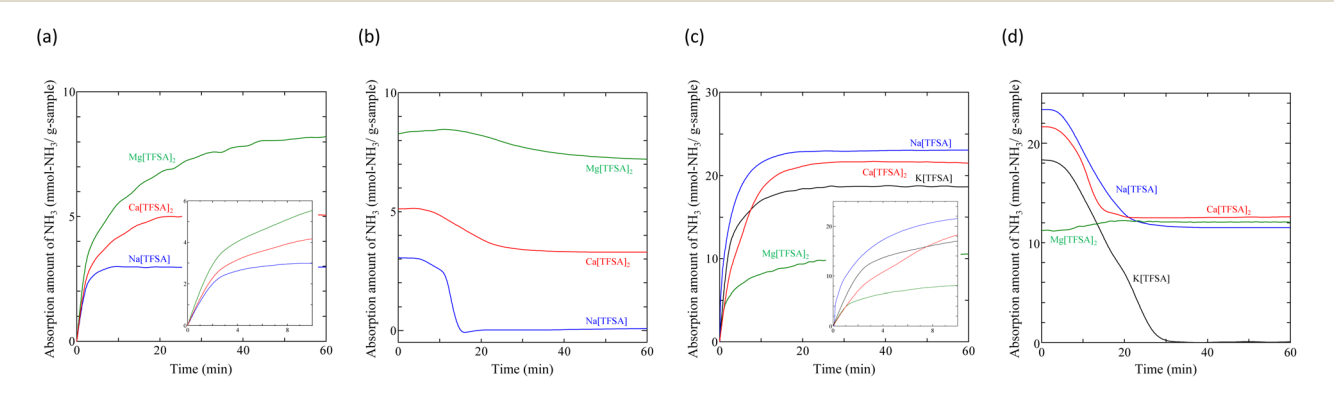


Fig. 11 Initial stages of NH_3 absorption/desorption of TFSA salts: (a) absorption at 473 K, (b) desorption at 473 K, (c) absorption at 300 K, and (d) desorption at 300 K.

Table 4 Kinetic parameters of NH₃ absorption into TFSA salts at 473 K

| TFSA | $A_{ m crd}$ | $A_{ m dis}$ | C | $k_{\mathrm{crd}}\times10^{-3}(\mathrm{s}^{-1})$ | $k_{\rm dis} \times 10^{-3} ({ m s}^{-1})$ | R^2 |
|-----------------------|--------------|--------------|----------|--|---|--------|
| Na[TFSA] | -2.13927 | -2.85738 | 4.996652 | 47.22 | 6.248 | 0.9994 |
| Mg[TFSA] ₂ | -3.44905 | -7.41104 | 10.86009 | 78.91 | 2.623 | 0.9994 |
| Ca[TFSA] ₂ | -2.75006 | -5.69369 | 8.44375 | 62.09 | 2.520 | 0.9991 |

Table 5 Kinetic parameters of NH₃ absorption into TFSA salts at 300 K

| TFSA | $A_{ m crd}$ | $A_{ m dis}$ | C | $k_{\mathrm{crd}}\times10^{-3}(\mathrm{s}^{-1})$ | $k_{\mathrm{dis}} \times 10^{-3} \left(\mathrm{s}^{-1} \right)$ | R^2 |
|-----------------------|--------------|--------------|----------|--|--|--------|
| Na[TFSA] | -10.4859 | -27.7007 | 38.1866 | 57.22 | 4.742 | 0.9999 |
| K[TFSA] | -16.5615 | -20.9808 | 37.5423 | 19.48 | 1.188 | 0.9997 |
| Mg[TFSA] ₂ | -7.29562 | -9.26933 | 16.54037 | 242.0 | 2.128 | 0.9967 |
| Ca[TFSA] ₂ | -7.03838 | -59.9431 | 66.89941 | 299.2 | 0.893 | 0.9996 |

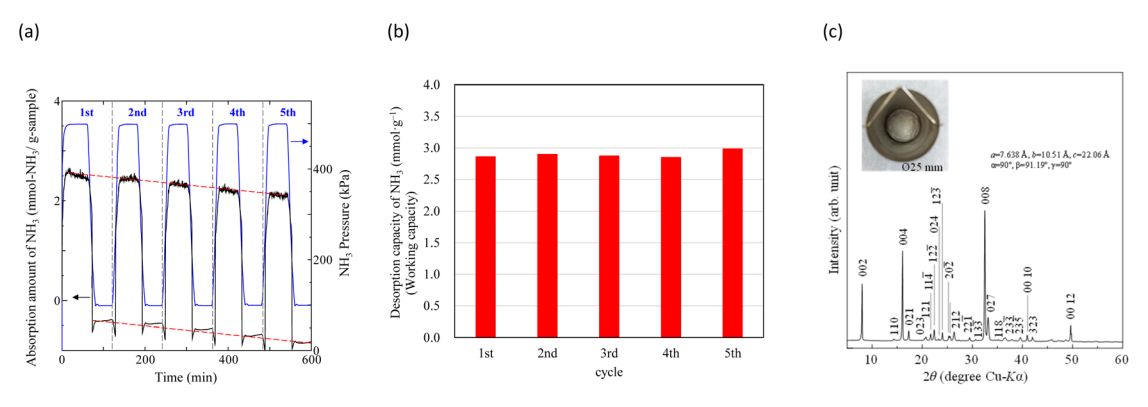


Fig. 12 The results of NH₃ absorption/desorption cycles (5 cycles) of Na[TFSA] at 473 K. (a) NH₃ absorption/desorption curves, (b) cycle performance of working capacity, and (c) the XRD pattern of the Na[TFSA] sample after five NH₃ absorption/desorption cycles

Conclusions

The NH₃ absorption and desorption behaviours of TFSA salts were investigated using PSA. The effects of the cation species and temperature on the NH3 absorption behaviour were evaluated for four TFSA salts: Na[TFSA], K[TFSA], Mg[TFSA]2, and Ca[TFSA]₂. NH₃ was absorbed by all of these solid TFSA salts. Among them, Na[TFSA] at 473 K and K[TFSA] at 300 K exhibited high NH₃ desorption ability, with NH₃ desorption capacities of 2.83 and 18.37 mmol g^{-1} and collection ratios of 93 and 99%, respectively. The NH3 absorption behaviour depended on the cation species of the TFSA salt. Crystallographic refinement showed that the crystal lattice of Na[TFSA] expanded and contracted along the c-axis during NH3 absorption and desorption, respectively, suggesting high desorption of NH₃ molecules from the lattice layers. For alkaline-earth metal TFSA salts, NH₄[TFSA] and amide compounds (Mg(NH₂)₂ or Ca(NH₂)₂) were formed after NH₃ absorption. This indicated that NH3 dissociated in solid TFSA salts. Therefore, two absorption processes, namely, coordination and dissociation of NH₃, occurred in the solid TFSA salts. Kinetic analysis confirmed that NH₃ dissociation was the rate-determining step for NH₃ storage in the salts.

Data availability

The data supporting this article have been included as part of the ESI.†

Author contributions

M. T.: investigation, data curation, visualization, writing original draft. R. F.: investigation, data curation. J. R.: supervision, funding acquisition, writing - review and editing, revision and suggestions. All the authors participated in discussions of the results and in preparing the manuscript.

Conflicts of interest

There are no conflicts to declare.

Acknowledgements

This research was supported by the Science and Technology Research Partnership for Sustainable Development (SATREPS) in collaboration with the Japan Science and Technology Agency (JST, JPMJSA2104) and the Japan International Cooperation

Agency (JICA). The authors gratefully acknowledge support provided by the Research Foundation. We would also like to thank Mr Shun Mashiko and Mr Morihiro Suzuki for their work on the preliminary experiments.

References

- 1 J. W. Erisman, M. A. Sutton, J. Galloway, Z. Klimont and W. Winiwarter, *Nat. Geosci.*, 2008, 1, 636.
- 2 A. Valera-Medina, H. Xiao, M. Owen-Jones, W. I. F. David and P. J. Bowen, *Prog. Energy Combust. Sci.*, 2018, **69**, 63.
- 3 K. E. Lamb, M. D. Dolan and D. F. Kennedy, *Int. J. Hydrogen Energy*, 2019, **44**, 3580.
- 4 D. R. MacFarlane, P.-V. Cherepanov, J. Choi, B. H. R. Suryanto, R. Y. Hodgetts, J. M. Bakker, F. M. F. Vallana and A. N. Simonov, *Joule*, 2020, 4, 1186.
- 5 M. Ravi and J. W. Makepeace, Chem. Sci., 2022, 13, 890.
- 6 S. Sun, Q. Jiang, D. Zhao, T. Cao, H. Sha, C. Zhang, H. Song and Z. Da, *Renewable Sustainable Energy Rev.*, 2022, **169**, 112918.
- 7 P. Mayer, A. Ramirez, G. Pezzella, B. Winter, S. M. Sarathy, J. Gascon and A. Bardow, *iScience*, 2023, **26**, 107389.
- 8 K. Aika, H. Hori and A. Ozaki, J. Catal., 1972, 27, 424.
- 9 K. Aika, Angew Chem. Int. Ed. Engl., 1986, 25, 558.
- 10 K. Aika and T. Kakegawa, Catal. Today, 1991, 10, 73.
- 11 K. Aika and H. Kobayashi, *CO*₂ *Free Ammonia as an Energy Carrier*, Springer, Singapore, 2023.
- 12 J. Guo and P. Chen, Chem, 2017, 3, 709.
- 13 Q. Wang, J. Guo and P. Chen, J. Energy Chem., 2019, 36, 25.
- 14 H. Liu, Chin. J. Catal., 2014, 35, 1619.
- 15 P. Wang, F. Chang, W. Gao, J. Guo, G. Wu, T. He and P. Chen, *Nat. Chem.*, 2016, **9**, 64.
- 16 R. Shi, X. Zhang, G. I. N. Waterhouse, Y. Zhao and T. Zhang, Adv. Energy Mater., 2020, 10, 2000659.
- 17 C. Y. Liu and K. Aika, Chem. Lett., 2002, 31, 798.
- 18 C. Y. Liu and K. Aika, Ind. Eng. Chem. Res., 2004, 43, 7484.
- 19 C. Y. Liu and K. Aika, Bull. Chem. Soc. Jpn., 2004, 77, 123.
- 20 C. Y. Liu and K. Aika, Ind. Eng. Chem. Res., 2004, 43, 6994.
- 21 C. Y. Liu and K. Aika, Res. Chem. Intermed., 2002, 28, 409.
- 22 C. Y. Liu and K. Aika, Bull. Chem. Soc. Jpn., 2003, 76, 1463.
- 23 C. Y. Liu and K. Aika, J. Jpn. Pet. Inst., 2003, 46, 301.
- 24 M. Malmali, Y. Wei, A. McCormick and E. L. Cussler, *Ind. Eng. Chem. Res.*, 2016, 55, 8922.
- 25 M. Malmali, G. Le, J. Hendrickson, J. Prince, A. V. McCormick and E. L. Cussler, ACS Sustainable Chem. Eng., 2018, 6, 6536.
- 26 M. Malmali, M. Reese, A. V. McCormick and E. L. Cussler, *ACS Sustainable Chem. Eng.*, 2018, **6**, 827.
- 27 C. Smith, M. Malmali, C. Liu, A. V. McCormick and E. L. Cussler, ACS Sustainable Chem. Eng., 2018, 6, 11827.
- 28 D. K. Ojha, M. J. Kale, A. V. McCormick, M. Reese, M. Malmali, P. Dauenhauer and E. L. Cussler, ACS Sustainable Chem. Eng., 2019, 7, 18785.
- 29 B. Lin, T. Wiesner and M. Malmali, ACS Sustainable Chem. Eng., 2020, 8, 15517.
- 30 B. Lin, F. H. Nowrin, J. J. Rosenthal, A. S. Bhown and M. Malmali, ACS Sustainable Chem. Eng., 2023, 11, 9880.

- 31 C. E. Onuoha, M. J. Kale, M. Malmali, P. J. Dauenhauer and A. V. McCormick, *Ind. Eng. Chem. Res.*, 2024, **63**, 5608.
- 32 E. W. Washburn, International Critical Tables of Numerical Data, Physics, Chemistry and Technology 7, McGraw-Hill, NY. 1929.
- 33 A. Yokozeki and M. B. Shiflett, *Ind. Eng. Chem. Res.*, 2007, 46, 1605.
- 34 T. Aoki, T. Ichikawa, H. Miyaoka and Y. Kojima, *J. Phys. Chem. C*, 2014, **118**, 8412.
- 35 Y. Kojima and M. Yamaguchi, *Int. J. Hydrogen Energy*, 2020, 45, 10233.
- 36 H. Chu, G. Wu, Z. Xiong, J. Guo, T. He and P. Chen, *Chem. Mater.*, 2010, 22, 6021.
- 37 M. J. Kale, D. K. Ojha, S. Biswas, J. I. Militti, A. V. McCormick, J. H. Schott, P. J. Dauenhauer and E. L. Cussler, ACS Appl. Energy Mater., 2020, 3, 2576.
- 38 C. Shen, P. Wang, L. Shen, X. Yin and Z. Miao, *Ind. Eng. Chem. Res.*, 2022, **61**, 8616.
- 39 W. Q. Gong, Y. X. Fu, Y. Zhou, M. S. Sun, Z. M. Li, N. H. Lu and D. J. Tao, Sep. Purif. Technol., 2023, 322, 124304.
- 40 K. Zong and D. Deng, Sep. Purif. Technol., 2024, 349, 127869.
- 41 Y. Cao, K. Jiang and D. Deng, Sustainable Energy Fuels, 2024, 8, 3933.
- 42 J. Foropoulos and D. D. DesMarteau, *J. Am. Chem. Soc.*, 1982, **104**, 4260.
- 43 J. Foropoulos and D. D. DesMarteau, *J. Fluorine Chem.*, 1982, 21, 9.
- 44 L. Xue, D. D. DesMarteau and W. T. Pennington, *Angew Chem. Int. Ed. Engl.*, 1997, **36**, 1331.
- 45 P. Johansson, S. P. Gejji, J. Tegenfeldt and J. Lindgren, *Electrochim. Acta*, 1998, 43, 1375.
- 46 A. Yokozeki and M. B. Shiflett, Appl. Energy, 2007, 84, 1258.
- 47 W. Shi and E. J. Maginn, AIChE J., 2009, 55, 2414.
- 48 J. Palomar, M. Gonzalez-Miquel, J. Bedia, F. Rodriguez and J. J. Rodriguez, *Sep. Purif. Technol.*, 2011, **82**, 43.
- 49 J. Bedia, J. Palomar, M. Gonzalez-Miquel, F. Rodriguez and J. J. Rodriguez, *Sep. Purif. Technol.*, 2012, **95**, 188.
- 50 Y. Li, M. C. Ali, Q. Yang, Z. Zhang, Z. Bao, B. Su, H. Xing and Q. Ren, *ChemSusChem*, 2017, **10**, 3368.
- 51 F. Zhong, H. Peng, D. Tao, P. Wu, J. Fan and K. Huang, *ACS Sustainable Chem. Eng.*, 2019, 7, 3258.
- 52 A. Finotello, J. E. Bara, D. Camper and R. D. Noble, *Ind. Eng. Chem. Res.*, 2007, **47**, 3453.
- 53 M. Ramdin, T. W. de Loos and T. J. H. Vlugt, *Ind. Eng. Chem. Res.*, 2012, **51**, 8149.
- 54 M. Ramdin, S. P. Balaji, J. M. Vicent-Luna, J. J. Gutiérrez-Sevillano, S. Calero, T. W. de Loos and T. J. H. Vlugt, *J. Phys. Chem. C*, 2014, **118**, 23599.
- 55 A. Rivera-Pousa, R. Lois-Cuns, M. Otero-Lema, H. Montes-Campos, T. Méndez-Morales and L. Miguel Varela, *J. Chem. Inf. Model.*, 2024, 64, 164.
- 56 L. Xue, D. D. DesMarteau and W. T. Pennington, *Solid State Sci.*, 2005, 7, 311.
- 57 K. Matsumoto, T. Matsui, T. Nohira and R. Hagiwara, J. Fluorine Chem., 2015, 174, 42.
- 58 L. Xue, C. W. Padgett, D. D. DesMarteau and W. T. Pennington, *Solid State Sci.*, 2002, **4**, 1535.

- 59 G. Veryasov, U. Harinaga, K. Matsumoto and R. Hagiwara, Eur. J. Inorg. Chem., 2017, 2017, 1087.
- 60 M. Tokushige, R. Fujisawa and J. Ryu, Sustainable Energy Fuels, 2024, 8, 397.
- 61 G. S. Pawley, J. Appl. Crystallogr., 1981, 14, 357.
- 62 H. Toraya, J. Appl. Crystallogr., 1986, 19, 440.
- 63 K. Momma and F. Izumi, J. Appl. Crystallogr., 2011, 44, 1272.
- 64 M. Tokushige and J. Ryu, ACS Omega, 2023, 8, 32536.
- 65 M. G. Davidson, P. R. Raithby, A. L. Johnson and P. D. Bolton, Eur. J. Inorg. Chem., 2003, 2003, 3445.

- 66 H. Jacobs, Z. Anorg. Allg. Chem., 1971, 382, 97.
- 67 L. Gao, H. Fang, Z. Li, X. Yu and K. Fan, Inorg. Chem., 2011, **50**, 4301.
- 68 R. Juza and H. Schumacher, Z. Anorg. Allg. Chem., 1963, 324,
- 69 N. Koga, Y. Goshi, S. Yamada and L. A. Pérez-Maqueda, J. Therm. Anal. Calorim., 2013, 111, 1463.
- 70 İ. Tosun, Int. J. Environ. Res. Public Health, 2012, 9, 970.
- 71 V. Kiss and K. Ősz, Int. J. Chem. Kinet., 2017, 49, 602.